LUND UNIVERSITY

Effect of covalent links on the structure, spectra, and redox properties of myeloperoxidase - A density functional study.

Devarajan, Ajitha; Gaenko, Alexander; Ryde, Ulf

Effect of covalent links on the structure, spectra, and redox properties of myeloperoxidase – a density functional study

Ajitha Devarajan [a,b], Alexander V. Gaenko [a,c], and Ulf Ryde [a*]

[a] Department of Theoretical Chemistry, Lund University, Chemical Center, P. O. Box 124, SE-221 00 Lund, Sweden.

[b] Chemistry Department, University of North Dakota, P. O. Box 9024, Grand Forks, ND 58201-9024, USA

[c] St. Petersburg State Institute of Technology (Technical University), Moskovskii av. 26, 190013, St. Petersburg, Russia

2017-03-19

---

*Correspondence to Ulf Ryde, E-mail: Ulf.Ryde@teokem.lu.se, Tel: +46 – 46 2224502, Fax: +46 – 46 2224543

Abstract

The enzyme myeloperoxidase shows several unusual properties compared to other peroxidases, e.g. a red-shifted absorption spectrum and a peroxidase activity towards chloride. It has been suggested that this is caused by the unusual covalent links between the heme group and the surrounding protein, but whether it is caused by the two ester links to Glu-242 and Asp-94 or the sulfonium ion linkage to Met-243 is unclear. To investigate these suggestions, we have used density functional theory to study the structure, spectra, and reduction potential of 25 models of myeloperoxidase in the reduced (Fe^{II}) and oxidized (Fe^{III}) states, as well as in the compound I (formally $Fe^{V}O$) and II ($Fe^{IV}O$ or $Fe^{IV}OH$) states, using appropriate models of the linkages to the Asp, Glu, and Met residues (including the back-bone connection between Glu-242 and Met-243) in varying combinations. The calculated spectral shifts indicate that both the ester and sulfonium linkages play a role in the spectral shift. On the other hand, the sulfonium linkage seems to be mainly responsible for the high positive reduction potential for both the ferric/ferrous and compound I/II couples of myeloperoxidase.

1. Introduction

The peroxidases constitute a big family of heme-containing enzymes that use H_2O_2 as an electron acceptor to catalyze a number of oxidative reactions. They are found in all types of organisms from bacteria to humans. Two superfamilies of peroxidases are normally distinguished [1]: The plant, fungal, and bacterial peroxidases are a big family of peroxidases that is genetically unrelated to the rather small family of mammalian peroxidases. One of the latter is myeloperoxidase (MPO, EC 1.11.1.7), which is present in high concentrations in the granules of phagocytic white blood cells [2]. There, it catalyzes the oxidation of chloride to hypochlorous acid, a potent bactericidal agent.

MPO is unusual in several different ways: First, it is the only mammalian peroxidase that peroxidizes chloride to hypochlorous acid at a substantial rate [3]. Second, MPO is green, whereas most other peroxidases are red or brown in color. This is caused by a relatively strong absorption band around 680 nm and a red-shift of the Soret band [2]. It is accompanied by a complicated resonance Raman spectrum and an inverted sign-pattern of the Soret band in the MCD spectrum [2]. Third, the heme group in MPO is connected to the surrounding protein by three unusual covalent crosslinks.

The X-ray crystal structure of human myeloperoxidase (MPO) was determined by Fielder et al. at 1.8 Å resolution [4]. The mature enzyme is a dimer of two identical subunits, each consisting of two polypeptide chains. The heme group in MPO is a derivative of protoporphyrin IX, in which the methyl groups on the pyrrole rings A and C form ester linkages to the carboxyl groups of Glu-242 and Asp-94, respectively. In addition, the β-carbon of the vinyl group on pyrrole ring A forms a sulfonium-ion linkage with the sulfur atom of Met-243. Similar ester linkages are found in three related mammalian peroxidases (eosinophil peroxidase, EPO, lactoperoxidase, LPO, and thyroid peroxidase, TPO), but the sulfonium-ion linkage appears to be unique to MPO [2]. The porphyrin ring in MPO is considerably distorted from planarity, having pyrrole ring A and, to a lesser extent ring C, tilted towards the distal side. The proximal heme ligand is the $N^{\varepsilon 2}$ atom of His-336. The distal heme cavity is occupied by Gln-91, His-95, Arg-239, and five water molecules. His-95 is hydrogen bonded to a water molecule that is positioned mid-way between the $N^{\varepsilon 2}$ atom and the heme iron ion. The Fe–O distance is ~2.9 Å, i.e. considerably longer than what is expected for a

typical sixth ligand. Consequently, the iron ion is in the high-spin state in the resting Fe^{III} form [2].

The reaction cycle of the heme peroxidases [5] starts with the resting Fe^{III} state. This state binds hydrogen peroxide, which is deprotonated to a hydroperoxide intermediate. When this intermediate is reprotonated on the distal oxygen atom, the O–O bond is cleaved in a heterolytic manner, resulting in water and compound I [6,7]. Formally, compound I is a $Fe^{V}O$ state, but one of the oxidizing equivalents is normally located in the porphyrin ring ($Fe^{IV}O$-porphyrin$^{+\bullet}$) [2,8]. However, Lardinois et al. [9] have observed an amino-acid radical in the EPR spectrum of at least one catalytic intermediate of MPO. This suggests that one of the oxidizing equivalent of compound I may be located on a nearby amino acid residue (corresponding to $Fe^{IV}O$-aa$^{+\bullet}$), as is also observed for some other peroxidases, e.g. cytochrome c peroxidase [5]. Although the $Fe^{IV}O$-porphyrin$^{+\bullet}$ and $Fe^{IV}O$-aa$^{+\bullet}$ states are isoelectronic, they are not expected to share the same spectra or redox properties.

Compound I is extremely reactive and can abstract an electron from almost any substrate. This results in the formation of a substrate radical and compound II ($Fe^{IV}O$), which does not react with halides [2]. Recent crystal structures and spectroscopic data have suggested that compound II in several other proteins is actually protonated and therefore is best described as $Fe^{IV}OH$ [10], although other investigations have questioned this interpretation [11]. $Fe^{IV}O$-aa$^{+\bullet}$ and $Fe^{IV}O$ differ only in the presence of protein radical, which is not expected to modify the absorption spectrum of the heme group significantly, and neither the Fe redox state nor the electronic configuration of the porphyrin ring are expected to change upon the conversion between these two intermediates.

The experimental absorption spectra of MPO in the Fe^{III} resting state is characterized by an intense Soret peak at 428–430 nm, with weaker peaks at 570, 620–625 and 690 nm and shoulders at 370 and 496 nm [1,2,6,7,12]. The former is strongly red-shifted, compared to the spectra of the other mammalian peroxidases (412–415 nm) [13,14], as well as of the plant peroxidases (~403 nm) [5]. The Soret band of the reduced enzyme is even more red shifted (472–474 nm compared to ~444 nm). It has been suggested that this change in the absorption spectrum may be caused by the covalent links between the heme group and the protein: Mutation of Met-243 in MPO into Thr, Gln and Val, which are corresponding residues in EPO, LPO, and

4

TPO, resulted in the shift of the Soret band in the Fe^{III} state to ~412 nm [13,14]. Likewise, the peak in the Fe^{II} state was shifted from 474 nm to ~446 nm. The mutants were unable to peroxidize chloride to hypochlorous acid, which was attributed to the sulfonium linkage, because the sulfur atom is expected to serve as an electron withdrawing substituent via its positive charge.

For the ester linkages, the results are more varying. Mutations of the Asp-94 residue in MPO to Asn or Val gave two species, one with spectral properties hardly affected from the wild type, whereas the other had strongly blue-shifted spectra (Soret bands at 413 and 444–445 nm for the Fe^{III} and Fe^{II} states, respectively) [15]. The latter form is believed to have lost the sulfonium ion linkage also. The Asp94Asn mutant retained ~30% of the chlorinating activity, but the Val mutant only ~5%. Mutation of the Glu-242 residue in MPO to Gln resulted in a blue-shift of the Soret band to 417–418 and 454–458 nm in the Fe^{III} and Fe^{II} states, respectively, and only 2–8% of the wild-type chlorinating activity [15-17]. The sulfonium ion linkage is believed to be intact in this mutant, but the heme group has become much more planar and symmetric.

The corresponding mutations in LPO have also been tested: The Asp225Val mutant had almost the same spectrum as the wild-type enzyme, whereas the Soret peak in the Fe^{III} form of the Glu375Gln mutant was blue-shifted by 5 nm (but the peak was still 5 nm red-shifted compared to fungal and plant peroxidases) [18]. However, both mutants had strongly reduced catalytic activities, especially for the physiological substrate thiocyanate.

In this paper we investigate the role of ester linkages on the absorption spectra of native and reduced enzyme and the role of sulfonium linkage on the spectra and redox potentials of MPO. We have used 25 models to describe the energetics, the electronic structure, as well as the spectral and redox properties of the enzyme in the reduced, oxidized, compound I, and II states. The effect of the back-bone connection between Glu-242 and Met-243 on the spectra was also considered, because it has been suggested to cause the distortion and the lowered symmetry of the heme ring in MPO [1]. Theoretical calculations can provide strong complementary information to the mutational data, because it is always clear exactly what structures and effects are studied, and the calculations directly sample the intrinsic effect of the crosslinks on the properties of the heme group, without any biasing effect of the surrounding

5

protein.

2. Methods

2.1 Computational details

Structures were optimized with density functional theory using the Becke–Perdew86 functional [19-23]. The calculations were sped up by expanding the Coulomb interactions in an auxiliary basis set, the resolution of identity (RI) approximation [24,25]. These calculations used the DZP basis [26] set for iron, enhanced with p, d, and f-type functions with exponents of 0.134915, 0.041843, 0.1244, and 1.339 (two p functions), and the 6-31G* basis set for all other atoms [27]. After the geometry optimization, the energies were recalculated with the B3LYP method and the same basis set [20-22,28,29], because this method is known to give more accurate energies for both small molecules and biochemical metal complexes [30-32]. Likewise, electronic spectra were calculated using time-dependent density functional theory (TD-DFT) with B3LYP functional and the same basis set. All calculations were carried out with the Turbomole software, version 5.7 [33-35].

The heme group without crosslinks was modeled as porphine (Por, i.e. the porphyrin ring without any side-chains) and the proximal histidine ligand was modeled by imidazole (Im). As mentioned above, the crystal structure of MPO shows a weakly bound water ligand (Fe–O distance ~2.9 Å) [2,4]. Therefore, we tested both five-coordinated models without and six-coordinated models with a water ligand. The ester linkages to Asp-94 and Glu-242 were modeled as acetate linkages (Por-CH_2-O-CO-CH_3) on pyrrole rings C and A (denoted Por-AG). The sulfonium linkage was modeled by Por-CH_2-CH_2-$S(CH_3)^+$-CH_2-CH_3 on ring A (called Por-M). The effect of including the protein back-bone connecting Glu-242 and Met-243 (Por-CH_2-O-CO-$(CH_2)_2$-CO-NH-$(CH_2)_3$-$S(CH_3)^+$-$(CH_2)_2$-Por) was also considered (called Por-AGMr). Compound I was modeled by ImPorFe^{V}O^{2-}, and compound II by either ImPorFe^{IV}O^{2-} or ImPorFe^{IV}OH$^-$, with or without the sulfonium ion linkage. The various models used in this investigation are shown in Figure 1.

To evaluate the extent of non-planarity of the porphyrin ring in the various models, the following approach was used. Initially, the geometric center of the four nitrogen atoms of the porphine unit was determined. Since these nitrogen atoms are not coplanar in general, two normal vectors for the planes containing two of the nitrogen atoms and the geometric center were constructed, and we let the average of these two normal vectors define the average plane. The direction of the normal vector was

7

chosen to be opposite to the direction of the axial imidazole ligand. The root-mean-squared distance of all atoms in the porphine ring, excluding the atoms of the side chains and hydrogen atoms, is denoted Por_{oop}. Likewise, Fe_{oop} is the distances of the iron ion from this plane.

When evaluating spin and charge distributions, we partitioned the models into the porphine ring, the Fe ion, the solvent molecule (H_2O, OH^-, or O^{2-}), the imidazole ring, and amino acid residues, denoted Asp, Glu and Met. Here, the Asp and Glu residues were $OCOCH_3$ and the Met residue was $S(CH_3)C_2H_5$, whereas the other parts of the side chains (CH_2 or CH_2-CH_2) were included in Por fragment. Spin densities and charges are also given for the N atoms of the Por ring (denoted N1 to N4, the O atom of the solvent ligand (O), the coordinating N atom of the Im ligand (N_{Im}), and the S atom in the Met linkage.

Transition metals with partly filled $3d$ orbitals can attain several spin states, low-spin (LS), intermediate-spin (IS) and high-spin (HS). We have studied the relative energy of the various spin states for all, and. the results are collected in Tables S1-3. The results are similar to what have been found in previous theoretical investigations of porphyrin models [36] and they do not change significantly when the crosslinks of the porphyrin ring are added. For most models, the results are in accordance with experimental observations [2,37], but for the Fe^{III} models and the five-coordinated Fe^{II} models, the stability of the IS state is overestimated, also if the B3LYP* method is used (in which the exact exchange contribution has been reduced from 0.20 to 0.15, thereby reducing the overstabilization of the higher spin states [38]) or if they are studied in a continuum solvent. This is a well documented shortcoming of the DFT calculations [36,39]. Therefore, we have concentrated on the experimental ground states of the various complexes, i.e. HS for the five-coordinated Fe^{II} and Fe^{III} states and IS for compounds I and II. In addition, we have also included the six-coordinated LS Fe^{II} and Fe^{III} states (with a water ligand) and the nearly degenerate LS state of compound I.

2.2 Solvation energies and redox potentials

Solvation energies were estimated using the continuum conductor-like screening model (COSMO) [40], as implemented in Turbomole [33-35]. In this method, the solute molecule forms a cavity within a dielectric continuum characterized by a

dielectric constant, ε. The charge distribution of the solute polarizes the dielectric medium and the response of the medium is described by screening charges on the surface of the cavity. Calculations were performed with the default parameters (implying a water-like probe molecule) and a dielectric constant of 4 and 80, to model possible effects in a protein (where the effective dielectric constant is normally estimated to be 2–40 [41-43]). For the generation of the cavity, the set of optimized radii in Turbomole 5.7 were used (H: 1.30 Å, C: 2.00 Å, N: 1.83 Å, O: 1.72 Å, S: 2.16 Å, Fe: 2.00 Å) [44].

Reduction potentials of the Fe^{III}/Fe^{II} and compound I/II couples were estimated from energies in a solvent according to

$$E^0 = E(ox) - E(red) - 4.43 \qquad (1)$$

where the term 4.43 eV represents the potential of the standard hydrogen electrode [45].

3. Results and Discussion

3.1 Geometries of the optimized models

We have studied the effect of the covalent crosslinks in MPO by optimizing the reduced Fe^{II} and oxidized Fe^{III} states (with and without an axial water molecule), as well as compounds I and II with different porphyrin models. The optimized geometries of all models are described in Table 1. They show that the $Fe–N_{Por}$ distances are are ~2.00 Å for all six-coordinated states (which are in the LS or IS states), but ~2.08 Å for the five-coordinated models (which are in the HS state). Likewise, the Fe ion is close to the center of the porphyrin plane in the former models (slightly shifted towards the axial imidazole ligand if the other axial ligand is water, but towards the oxygen ligand in the models of compounds I and II), but it is distinctly out of the porphyrin plane (towards the imidazole ligand) in the five-coordinated models (by 0.26–0.40 Å). The $Fe–N_{Im}$ distance is 1.94 Å in the $Fe^{II/III}H_2O$ states, 2.05 Å for the protonated compound II model, and 2.09–2.17 Å for the other states. This is similar to what has been observed in previous theoretical investigations [36]. The various crosslinks have only a minimal effect on the Fe–ligand and Fe_{oop} distances.

We have estimated the general distortion of the porphyrin ring by the root-mean-

square displacement of all atoms of the porphyrin from the average plane (Por_{oop}). From Table 1, it can be seen that the porphyrin ring is more distorted in the Fe^{III} state than in the reduced state and even more distorted in compound I and protonated compound II. Moreover, the distortion in compound I is larger in the IS than in the LS state. In general, the ester and sulfonium linkages increase the distortion of the porphine unit, but the effect is rather small.

As discussed above, the resting form of MPO is in the HS Fe^{III} state. The crystal structure of this state shows a water molecule at a Fe–O distance of 2.90 Å [4]. This is much longer than in any of the optimized ground states (~2.10 Å for Fe^{II}–H_2O, ~2.05 Å for Fe^{III}–H_2O, ~1.64 Å for compound I and deprotonated compound II, and 1.78 Å for protonated compound II) and even longer than in HS six-coordinated $Fe^{III}H_2O$ models (2.33–2.45 Å). This shows that this sixth ligand in the crystal structure is non-bonding, with a position that is stabilized by interactions to the surrounding protein (especially by His-95).

The crystal structure shows clear signs of the HS Fe^{III} state with the Fe ion 0.32 Å below the porphyrin plane and Fe–N_{Por} and Fe–N_{Im} distances of 1.99 and 2.19 Å. The corresponding values in the optimized HS Fe^{III} models are around 0.39, 2.08, and 2.10 Å, which are reasonable considering the accuracy of the crystal structure (~0.1 Å [46,47]) and the theoretical calculations (~0.05 Å [48]). However, the distortion of the porphyrin ring is larger in the crystal structure than in the optimized models (Por_{oop} is 0.28 Å compared to 0.08 Å). This shows that the protein surrounding is more important for this distortion than the linkages and their connecting backbone (as in the AGMr model).

3.2 Spin densities and Mulliken charges

Spin densities of selected atoms and groups in the the various models are shown in Table 2. The spin densities are similar to what have been observed for the same states in other porphyrin models before [36]: The Fe^{II} and $Fe^{II}I$ models have the spin concentrated on the metal, compound I is essentially Fe^{III}–$Por^{\bullet}$–$O^{-\bullet}$, deprotonated compound II is Fe^{III}–$O^{-\bullet}$, whereas protonated compound II is an almost pure Fe^{IV}–OH^- state. Interestingly, in all cases, the effect of the ester or sulfonium linkages on spin density distributions is minimal. In particular, no spin density is seen on the ester or sulfonium ion linkages.

Mulliken charges on selected atoms and groups for all models are given in Table 3. It can be seen that there is no effect from the ester and sulfonium linkages on the charges of the Fe ion, the Im group, or the O-ligand. However, there is a redistribution of the charge of porphine ring from the Por core of the ring to the crosslinks: The ester linkages reduce the negative charge of porphine core by 0.5 e and the sulfonium linkage reduces it by an additional 0.2 e, in an almost additive manner. The picture remains the same when the oxidation state of the metal changes.

3.3 Absorption spectra

We have calculated the absorption spectra of the various models with the TD-DFT method. The calculated spectrum for the Fe^{III} resting state of the Por-AGM model is shown in Figure 2 (pink bars). It can be seen that it consists of a number of rather intense peaks around 370 nm. All these peaks add to a single broad absorption band with the maximum at 367 nm if a Gaussian distribution is added to each peak (with a peak half-width of 2500 cm^{-1}; similar results are obtained with other values).

This corresponds to the intense Soret band in the experimental spectrum of MPO, which is observed at 428–430 nm [1,2,6,7,12]. Thus, the absorption maximum is calculated at a 61–63 nm too low wavelength. This is caused by shortcomings in the theoretical method, e.g. the rather small basis sets and the omission of the porphyrin side chains. However, these shortcomings are the same in all calculations and the shift can therefore be expected to be the same in all calculations. This is confirmed in the calculation on the reduced Fe^{II}(Por-AGM)Im model, which gives an absorption maximum at 412 nm, which is 60–62 nm lower than the experimental value of 472–474 nm [1,2,6,7,12]. Therefore, we can expect that the differences between the various models will reproduce experimental spectral shifts quite accurately.

We have systematically investigated the effect of the ester and sulfonium ion crosslinks of the porphyrin ring on the absorption spectra. From Figure 2 and Table 4, it can be seen that removing the sulfonium ion linkage from the Por-AGM model (yielding the Por-AG model) leads to a blue-shift of the calculated spectrum by 22 and 5 nm for the Fe^{II} and Fe^{III} states, respectively. This is in reasonable agreement with the experimental spectra of other mammalian peroxidases (blue shifts of ~29 and 17 nm, respectively) [13,14]. If we instead remove the ester linkages, the spectra are blue-shifted by 26 and 13 nm, respectively. Interestingly, the effects of the two types

of groups are essentially additive, so the removal of both the ester and sulfonium ion linkages blue-shifts the spectra by 56 and 17 nm, respectively. These results are quite similar to the experimental evidence based on native and mutant enzymes [10-16].

In these comparisons, it can be argued that we ignored the effect of the vinyl group before it reacts with Met-234. Therefore, we have also performed a set of calculations with the Por model extended with a vinyl groups. However, this changed the absorption maximum by only 2 nm. Likewise, a sixth water ligand had only minor effects on the spectrum of the Fe^{II} and Fe^{III} models.

We have also studied the spectra of compounds I and II. The calculated spectrum of compound I is red-shifted by 20 nm compared to the spectra of the Fe^{III} model. These calculations were performed on the IS state on the Por-M model, but the results with the LS state are similar. Experimentally, compound I in MPO absorbs at 425 nm (i.e. red-shifted by ~4 nm compared to the ferric resting state) with a 50% lower intensity than the Fe^{III} resting state [2]. Thus, in this case, the calculated spectral shifts trends do not agree so well with the experimental ones; however, the integral intensity of the compound I model peak (~0.5) is roughly 50% of the integral intensity of the resting state model peak (~1.1).

On the other hand, the calculated spectrum of compound II is red shifted by 23 nm, which is in good agreement with an experimentally observed shift of ~26 nm [2]. This shows quite strongly that it is unlikely that the extra unpaired electron in compound I is on a nearby amino acid in MPO (which would give similar spectra for compounds I and II).

Finally, we note that we have a similar problem with the spectrum of compound I without the sulfonium linkage (i.e. the Por model of plant peroxidases): Also for this model, we calculate a red-shift of the compound I model, compared to the resting Fe^{III} state, whereas experiments indicate a blue-shift of 3 nm. On the other hand, we calculate a red-shift of 23 nm for the unprotonated compound II model, in good agreement with the observed 17 nm shift [5]. For the protonated compound II model, the red shift is 19 nm. Unfortunately, the differences in the shifts are too small (compared to the accuracy of these calculations) to decide whether the oxygen ligand in compound II is protonated or not.

3.4 Reduction potentials

In order to understand the structure–function relationships of heme peroxidases, we have also calculated the reduction potentials of the various models. In redox-potential calculations, solvation energies are as important as the electronic energies. These have been estimated by the COSMO continuum model, with three different values of the dielectric constant (1, 4, and 80) to model possible effects of the surrounding protein (the effective dielectric constant of a protein has been estimated to be 2–40 [41-43]). The redox potentials of the various redox couples, calculated with Eqn. 1, are presented in Table 5.

It can be seen that the reduction potentials strongly depend on the dielectric constant. For example, we predict a $Fe^{II/III}$ reduction potential for the five-coordinated MPO model ($Fe^{II/III}$Por-AGM) of 0.9 V with $\varepsilon = 4$ and –0.03 V with $\varepsilon = 80$. Naturally, this crude continuum model, without any atomic details of the surrounding protein, cannot exactly reproduce experimental data. However, it is quite satisfactorily that the measured value, 0.025 V [1], is within this calculated range.

The potential of the Por-AGM model is appreciably more positive than that of the other porphyrin models: Removing the sulfonium ion linkage (Por-AG), gives a reduction potential of 0.18 to –0.16 V ($\varepsilon = 4$ and 80). This time, the measured potential for LPO, –0.19 V [1], is just outside this range. The reason for this is probably that the five-coordinated models ignore the sixth, weak water ligand. From Table 5, it can be seen that the six-coordinated models give 0.2–0.4 V more negative potentials (because a sixth ligand will stabilize the oxidized state). Thereby, the measured LPO and MPO potentials fall well inside the calculated range (and close to the $\varepsilon = 4$ limit). Surely, a six-coordinated model overestimates the effect of the axial ligand, but apparently, the five-coordinated model underestimates it, and the truth fall in between.

If also the ester linkages are removed (yielding the Por model), the calculated potential is even more negative, 0.04 to –0.31 V (for the five-coordinated model), although the effect is appreciably smaller than for the sulfonium ion linkage. Again, this is similar to what is found for plant peroxidases, e.g. –0.22 V for horseradish peroxidase [5].

We have also studied the reduction potential of the compound I/II couple. It is appreciably more positive than for the $Fe^{II/III}$ couple. For the MPO model, it is 1.6–0.7 V ($\varepsilon = 4$ and 80), i.e. reasonably close to the experimental estimate of 1.35 V [1].

Again, the effect of the crosslinks are appreciable: The calculated potential of the Por model is 0.9–0.6 V and the experimental value for horseradish peroxidase is 0.897 V [5]. Thus, our results clearly show that covalent crosslinks of the mammalian peroxidases have a strong influence on their reduction potentials, making them more positive. Moreover, the effect is larger for the sulfonium ion linkage than for the ester linkages. This provides a plausible explanation why MPO is the only peroxidase that can peroxidize chloride to hypochlorous acid at a substantial rate.

4. Conclusions

In order to understand the unusual spectral and catalytic properties of MPO, we have investigated 25 models representing the various states of MPO. We have studied how the ester and sulfonium linkages affect the geometry, electronic structure, spectra and the redox potentials of the models.

The ester and sulfonium linkages have little influence on the spin density and geometry of the models and they do not change the preferred spin states. They have a small influence on the distortion of the porphyrin ring, but the effect of the surrounding protein seems to be more important. However, the linkages have quite extensive influence on the spectra: Both linkages cause a red-shift of the Soret band of the spectrum and the two shifts are almost additive. Calculated shifts corresponding to the various mutations and red shift for compound II agree well with the experimental values.

Finally, we have calculated reduction potentials for the $Fe^{II/III}$ and compound I/II redox couples and show that both linkages make the reduction potentials more positive, although the effect of the sulfonium linkage is appreciably larger than that of the ester linkages. This indicates that the reactivity of MPO against Cl^- is an effect of this increase in the reduction potential, caused by the sulfonium linkage.

5. Abbreviations

aa = amino acid

COSMO = continuum conductor-like screening model

DFT = density functional theory

EPO = eosinophil peroxidase

HS = high spin; Im = imidazole

IS = intermediate spin

LPO = lactoperoxidase

LS = low spin

MPO = myeloperoxidase

Por = porphine

RI = resolution of the identity

TD-DFT = time-dependent DFT

TPO = thyroid peroxidase

6. Acknowledgments

References

[1] P.G. Fortmüller, M. Zederbauer, W. Jantschko, J. Helm, M. Bogner, C. Jakopitsch, C. Obinger, Arch. Biochem. Biophys. 445 (2006) 199-213.

[2] R.E. Fenna, in: A. Messerschmidt, R. Huber, T. Poulos, K. Wieghardt (eds) Handbook of metalloproteins, Vol. 1, J. Wiley and Sons, Chichester, 2001, pp. 211-221.

[3] J.E. Harrison, J. Schultz, J. Biol. Chem. 251 (1976) 1371-1374.

[4] T.J. Fielder, C. A. Davey, R.E. Fenna, J. Biol. Chem. 275 (2000) 11964-11971.

[5] M. Gajhede, in: A. Messerschmidt, R. Huber, T. Poulos, K. Wieghardt (eds) Handbook of metalloproteins, Vol. 1, J. Wiley and Sons, Chichester, 2001, pp. 195-209.

[6] J.E. Harrison, T. Araiso, M. Palcic, H. B. Dunford, Biochem. Biophys. Res. Comm. 94 (1980) 34-40.

[7] J.E. Svensson, K. Domeji, S. Lindvall, G. Rydell, Biochem. J 242 (1980) 673-6800.

[8] E. Ghibaudi, E. Laurenti, Eur. J. Biochem. 270 (2003) 4403-4412.

[9] O.M. Lardinois, P.O. de Montellano, Biochem. Biophys. Res. Comm 270 (2000) 199-202.

[10] H.-P. Hersleth, U. Ryde, P. Rydberg, C.H. Görbitz, K.K. Andersson, J. Inorg. Biochem. 100 (2006) 460-476.

[11] R.K. Behan, M.T. Green, J. Inorg. Biochem. 100 (2006) 448-459.

[12] L.A. Marquez, J.T. Huang, H.B. Dunford, Biochemistry 33 (1994) 1447-1454.

[13] I.M. Kooter, N. Moguilevsky, A. Bollen, N.M. Sijtsema, C. Otto, R. Wever, J. Biol. Inorg. Chem 2 (1997) 191-197.

[14] I.M. Kooter, N. Moguilevsky, A. Bollen, L.A. van der Veen, C. Otto, H.I. Dekker, R. Wever, J. Biol. Chem. 274 (1999) 26794-26802.

[15] I.M. Kooter, N. Moguilevsky, A. Bollen, N.M. Sijtsema, C. Otto, H.I. Dekker, R. Wever, Eur. J. Biochem. 264 (1999) 211-217.

[16] R. Floris, N. Moguilevsky, T. Puppels, A. Jacquet, R. Renire, A. Bollen, R. Wever, J. Am. Chem. Soc. 117 (1995) 3907-3912.

[17] M. Zederbauer, W. Jantschko, K. Neugschwandtner, C. Jakopitsch, N. Moguilevsky, C. Obinger, P.G. Fortmüller, Biochem. 44 (2005) 6482-6491.

[18] G. Suriano, S. Watanabe, E.M. Ghibaudi, A. Bollen, R.P. Ferrari, N.

Moguilevsky, Bioorg. Med. Chem. Lett. 11 (2001) 2827-2831.

[19] J.P. Perdew, Phys. Rev. B 33 (1986) 8822-8824.

[20] P.A.M. Dirac, Proc. Royal Soc. (London) A 123 (1929) 714.

[21] J.C. Slater, Phys. Rev. 81 (1951) 385-390.

[22] S. Vosko, L. Wilk, M. Nussair, Can. J. Phys.58. (1980)1200.

[23] A.D. Becke, Phys. Rev. A 38 (1988) 3098.

[24] K. Eichkorn, O. Treutler, H. Öhm, M. Häser, R. Ahlrichs, Chem. Phys. Lett., 240 (1995) 283-290.

[25] K. Eichkorn, F. Weigend, O. Treutler, R. Ahlrichs Theor. Chem. Acc. 97 (1997) 119-126.

[26] A. Schäfer, H. Horn, R. Ahlrichs, J. Chem. Phys. 97 (1992) 2571.

[27] W.J. Hehre, L. Radom, P.v.R. Schleyer, J.A. Pople In Ab initio molecular orbital theory, Wiley-Interscience, New York, 1986

[28] A.D. Becke, J. Chem. Phys. 98 (1993) 5648.

[29] C. Lee, W. Yang, R.G. Parr, Phys. Rev. B 37 (1988) 785.

[30] C.W. Bauschlicher, Chem. Phys. Lett. 246 (1995) 40-44.

[31] P.E.M. Siegbahn, J. Biol. Inorg. Chem. 11 (2006) 695-701.

[32] F. Neese, J. Biol. Inorg. Chem. 11 (2006) 702-711.

[33] F. Furche, R. Ahlrichs, J. Chem. Phys. 117 (2002) 7433-7447.

[34] H. Weiss, R. Ahlrichs, M. Häser, J. Chem. Phys. 99 (1993) 1262-1270.

[35] O. Treutler, R. Ahlrichs, J. Chem. Phys. 102 (1995) 346-354.

[36] P. Rydberg, E. Sigfridsson, U. Ryde, J. Biol. Inorg. Chem 9 (2004) 203-223.

[37] S. Seibold, J.F. Cerda, A.M. Mulichak, I. Song, M. Garavito, T. Arakawa, W.L. Smith, G.T. Babcock, Biochemistry 39 (2000) 6616-6624.

[38] M. Reiher, O. Salomon, B.A. Hess, Theor. Chem. Acc. 107 (2001) 48-55.

[39] C. Rovira, K. Kunc, P. Hutter, P. Ballone, M. Parrinello, J. Phys. Chem. A 101 (1997) 8914-8925.

[40] A. Klamt, J. Schüürmann, J. Chem. Soc. Perkin Trans 2 (1993) 799.

[41] K. A. Sharp, Annu. Rev. Biophys. Biophys. Chem. , 19 (1990) 301

[42] B. Honig, A. Nicholls, Science, 268 (1995) 1144.

[43] C.N. Schutz, A. Warshel, Proteins, Struct. Funct. Genet. 2001, 44, 400-417.

[44] A. Klamt, V. Jonas, T. Bürger, J.C.W. Lohrenz J. Phys. Chem. 102 (1998) 5074-5085.

[45] H. Reiss, A. Heller, J. Phys. Chem., 89 (1985) 4207

[46] B.A. Fields, H.H. Bartsch, H.D. Bartunik, F. Cordes, J.M. Guss, H.C. Freeman, Acta Crystallogr. D 50 (1994) 709-730,

[47] D.W.J. Cruickshank, Acta Crystallogr. D 55 (1999) 583-601.

[48] U. Ryde, K. Nilsson, J. Am. Chem. Soc. 2003, 125, 14232-14233, Y. Shen & U. Ryde (2004) J. Inorg. Biochem., 98, 878-895.

Table 1. Optimized geometry parameters of the MPO models.

Model	Multiplicity	Fe—N_{avg}	Fe—N_{Im}	Fe—O	Fe_{oop}	Por_{oop}
Fe^{II}	5	2.08	2.15		-0.26	0.07
Fe^{II}-AG	5	2.08	2.15		-0.29	0.08
Fe^{II}-AGM	5	2.09	2.14		-0.31	0.09
Fe^{II}-AGMr	5	2.08	2.15		-0.29	0.06
Fe^{II}-M	5	2.09	2.14		-0.31	0.10
$Fe^{II}H_2O$	1	2.00	1.94	2.10	-0.06	0.04
$Fe^{II}H_2O$-AG	1	2.00	1.94	2.10	-0.06	0.05
$Fe^{II}H_2O$-AGM	1	2.00	1.94	2.10	-0.06	0.04
$Fe^{II}H_2O$-AGMr	1	2.00	1.94	2.10	-0.06	0.04
$Fe^{II}H_2O$-M	1	2.00	1.94	2.10	-0.06	0.04
Fe^{III}	6	2.07	2.10		-0.38	0.08
Fe^{III}-AG	6	2.07	2.11		-0.37	0.08
Fe^{III}-AGM	6	2.08	2.10		-0.39	0.12
Fe^{III}-AGMr	6	2.07	2.10		-0.38	0.08
Fe^{III}-M	6	2.08	2.09		-0.40	0.09
$Fe^{III}H_2O$	2	2.00	1.94	2.04	-0.07	0.09
$Fe^{III}H_2O$-AG	2	2.00	1.94	2.05	-0.07	0.06
$Fe^{III}H_2O$-AGM	2	2.01	1.94	2.06	-0.07	0.07
$Fe^{III}H_2O$-AGMr	2	2.01	1.94	2.05	-0.07	0.07
$Fe^{III}H_2O$-M	2	2.00	1.94	2.06	-0.07	0.10
$Fe^{IV}O$	3	2.02	2.17	1.65	0.10	0.06
$Fe^{IV}O$-M	3	2.02	2.16	1.65	0.09	0.11
$Fe^{IV}OH$	3	2.00	2.05	1.78	0.05	0.14
$Fe^{V}O$	2	2.02	2.12	1.63	0.10	0.14
$Fe^{V}O$-M	2	2.01	2.12	1.63	0.09	0.19
$Fe^{V}O$	4	1.99	2.13	1.65	0.08	0.29
$Fe^{V}O$-M	4	1.99	2.13	1.65	0.08	0.31
$Fe^{III}H_2O$	Crystal	1.99	2.19	2.90	-0.32	0.28

Table 2. Spin densities of selected atoms and groups in the various MPO models.

Model	Multiplicity	Fe	Por	H_2O	Im	Asp	Glu	Met	N1	N2	N3	N4	O	N_{Im}
Fe^{II}	5	3.81	0.15		0.04				0.04	0.04	0.04	0.04		0.05
Fe^{II}-AG	5	3.80	0.15		0.05	0.00	0.00		0.04	0.05	0.04	0.05		0.04
Fe^{II}-AGM	5	3.81	0.14		0.05	0.00	0.00	0.00	0.05	0.04	0.05	0.04		0.04
Fe^{II}-M	5	3.80	0.15		0.05			0.00	0.04	0.05	0.04	0.05		0.04
Fe^{II}-AGMr	5	3.80	0.15		0.05	0.00	0.00	0.00	0.04	0.05	0.04	0.05		0.04
Fe^{III}	6	4.19	0.70		0.11				0.13	0.13	0.13	0.13		0.09
Fe^{III}-AG	6	4.19	0.70		0.11	0.00	0.00		0.13	0.13	0.13	0.13		0.09
Fe^{III}-AGM	6	4.19	0.70		0.11	0.00	0.00	0.00	0.13	0.12	0.13	0.14		0.09
Fe^{III}-M	6	4.19	0.69		0.12			0.00	0.13	0.12	0.13	0.14		0.09
Fe^{III}-AGMr	6	4.19	0.74		0.09	0.00	0.00	0.00	0.13	0.12	0.13	0.14		0.09
$Fe^{III}H_2O$	2	1.03	-0.01	0.00	-0.02				-0.02	-0.02	-0.02	-0.02	0.00	-0.03
$Fe^{III}H_2O$-AG	2	1.04	-0.03	0.00	-0.01	0.00	0.00		-0.02	-0.02	-0.02	-0.02	-0.01	-0.04
$Fe^{III}H_2O$-AGM	2	1.04	-0.03	-0.01	-0.01	0.00	0.00	0.00	-0.02	-0.02	-0.02	-0.02	-0.01	-0.03
$Fe^{III}H_2O$-M	2	1.04	-0.03	-0.01	0.00			0.00	-0.02	-0.02	-0.02	-0.02	-0.01	-0.03
$Fe^{IV}O$	3	1.14	-0.06		-0.01				0.00	0.00	0.00	0.00	0.93	-0.01
$Fe^{IV}O$-M	3	1.14	-0.06		-0.01			0.00	0.00	0.00	0.00	0.00	0.93	-0.01
$Fe^{IV}OH$	3	1.83	-0.02		-0.01				-0.03	0.01	-0.03	-0.04	0.19	-0.02
$Fe^{V}O$	2	1.13	-1.04		-0.03				-0.15	-0.15	-0.14	-0.14	0.94	-0.04
$Fe^{V}O$	4	1.10	0.92		0.01				0.15	0.14	0.15	0.14	0.97	0.00
$Fe^{V}O$-M	2	1.13	-1.04		-0.03			0.00	-0.14	-0.14	-0.15	-0.16	0.94	-0.04
$Fe^{V}O$-M	4	1.10	0.91		0.01			0.00	0.14	0.15	0.14	0.15	0.97	0.00

Table 3. Mulliken charges of selected atoms and groups in the various MPO models.

Model	Multiplicity	Fe	Por	H_2O	Im	Asp	Glu	Met	N1	N2	N3	N4	O	N_{Im}	S
Fe^{II}	5	0.84	-0.98		0.14				-0.60	-0.61	-0.61	-0.60		-0.44	
Fe^{II}-AG	5	0.84	-0.42		0.16	-0.29	-0.29		-0.63	-0.60	-0.63	-0.60		-0.45	
Fe^{II}-AGM	5	0.85	-0.26		0.18	-0.28	-0.26	0.76	-0.60	-0.64	-0.60	-0.64		-0.46	0.53
Fe^{II}-M	5	0.85	-0.81		0.18			0.79	-0.62	-0.60	-0.62	-0.59		-0.46	0.54
Fe^{II}-AGMr	5	0.84	-0.26		0.17	-0.28	-0.17	0.70	-0.62	-0.60	-0.62	-0.60		-0.45	0.59
$Fe^{II}H_2O$	1	0.61	-0.92	0.17	0.14				-0.54	-0.56	-0.56	-0.54	-0.76	-0.43	
$Fe^{II}H_2O$-AG	1	0.62	-0.33	0.18	0.14	-0.30	-0.30		-0.54	-0.56	-0.56	-0.55	-0.76	-0.43	
$Fe^{II}H_2O$-AGM	1	0.63	-0.17	0.17	0.16	-0.28	-0.26	0.76	-0.54	-0.56	-0.56	-0.55	-0.75	-0.43	0.53
$Fe^{II}H_2O$-M	1	0.62	-0.73	0.17	0.16			0.78	-0.54	-0.55	-0.56	-0.54	-0.75	-0.43	0.54
Fe^{III}	6	1.00	-0.27		0.26				-0.62	-0.63	-0.63	-0.62		-0.51	
Fe^{III}-AG	6	1.00	0.25		0.26	-0.26	-0.26		-0.63	-0.64	-0.63	-0.63		-0.51	
Fe^{III}-AGM	6	1.02	0.32		0.27	-0.24	-0.21	0.84	-0.64	-0.64	-0.64	-0.64		-0.52	0.56
Fe^{III}-M	6	1.02	-0.16		0.28			0.85	-0.64	-0.63	-0.64	-0.63		-0.52	0.56
Fe^{III}-AGMr	6	1.01	0.36		0.27	-0.25	-0.15	0.75	-0.63	-0.64	-0.63	-0.64		-0.51	0.58
$Fe^{III}H_2O$	2	0.81	-0.30	0.21	0.27				-0.58	-0.57	-0.58	-0.56	-0.75	-0.47	
$Fe^{III}H_2O$-AG	2	0.82	0.22	0.21	0.28	-0.26	-0.26		-0.57	-0.58	-0.58	-0.59	-0.75	-0.47	
$Fe^{III}H_2O$-AGM	2	0.82	0.34	0.21	0.30	-0.25	-0.23	0.82	-0.57	-0.58	-0.58	-0.58	-0.75	-0.47	0.55
$Fe^{III}H_2O$-M	2	0.82	-0.18	0.21	0.30			0.85	-0.57	-0.58	-0.58	-0.57	-0.75	-0.47	0.56
$Fe^{IV}O$	3	0.83	-0.57		0.17				-0.54	-0.54	-0.54	-0.54	-0.44	-0.40	
$Fe^{IV}O$-M	3	0.83	-0.38		0.19			0.80	-0.54	-0.55	-0.54	-0.54	-0.44	-0.40	0.54
$Fe^{IV}OH$	3	0.91	-0.01		0.30				-0.56	-0.58	-0.55	-0.56	-0.65	-0.43	
$Fe^{V}O$	2	0.85	0.33		0.24				-0.53	-0.54	-0.51	-0.51	-0.41	-0.41	
$Fe^{V}O$	4	0.85	0.31		0.24				-0.52	-0.53	-0.52	-0.53	-0.40	-0.41	
$Fe^{V}O$-M	2	0.85	0.45		0.25			0.86	-0.52	-0.51	-0.53	-0.54	-0.41	-0.42	0.56
$Fe^{V}O$-M	4	0.85	0.44		0.26			0.86	-0.52	-0.53	-0.52	-0.52	-0.40	-0.42	0.56

Table 4. Absorption maxima (nm) of the various MPO models. The spectral shifts are relative to the Por-AGM model for the $Fe^{II/III}$ states, but relative to the Fe^{III} state for compounds I and II. Experimental data from [1,2,6,7,10-16].

Model	Maxima	shift	Maxima (exp)	shifts (exp)
Fe^{II}	308,356*	56	437	35–37
Fe^{II}-AG	321,390*	22	444–445	27–30
Fe^{II}-M	340,386*	26	458	14–16
Fe^{II}-AGM	330,412*	0	472–474	0
Fe^{III}	350	17	403	25–27
Fe^{III}-AG	362	5	412–415	13–18
Fe^{III}-M	354	13	418	10–12
Fe^{III}-AGM	367	0	428–430	0
Fe^{III}	350	0	403	0
$Fe^{IV}O(IS)$	373	23	420	17
$Fe^{IV}OH(IS)$	369	19	420	17
$Fe^{V}O(IS)$	370	20	400	-3
Fe^{III}-M	354	0	428	0
$Fe^{IV}O$-M(IS)	377	23	455	27
$Fe^{V}O$-M(IS)	374	20	425	-3

* The most intense peak

Table 5. Redox potentials of the various MPO models in mV. Experimental data from [1,5].

Model	Vac.	$\varepsilon = 4$	$\varepsilon = 80$	Experiment
		Fe^{III}/Fe^{II}		
Por	843	44	-310	-220
Por-AG	935	183	-157	-190
Por-M	2799	738	-194	
Por-AGM	3002	929	-30	25
		$Fe^{III}H_2O/Fe^{II}H_2O$		
Por	692	-164	-554	-220
Por-AG	684	-152	-543	-190
Por-M	2559	421	-560	
Por-AGM	2588	494	-478	25
		$Fe^{V}O/Fe^{IV}O$		
Por	1717	952	626	897
Por[a]	1683	914	586	
Por-M	3663	1596	668	1350
Por-M[a]	3659	1591	659	

[a]Low-spin state

23

Figure legends

Figure 1. Optimized structures of the $Fe^{II/III}$, $Fe^{II/III}$-AG, $Fe^{II/III}$-AGM, $Fe^{II/III}H_2O$, $Fe^{II/III}H_2O$-AGMr, $Fe^{IV/V}O$, and $Fe^{IV}OH$ models.

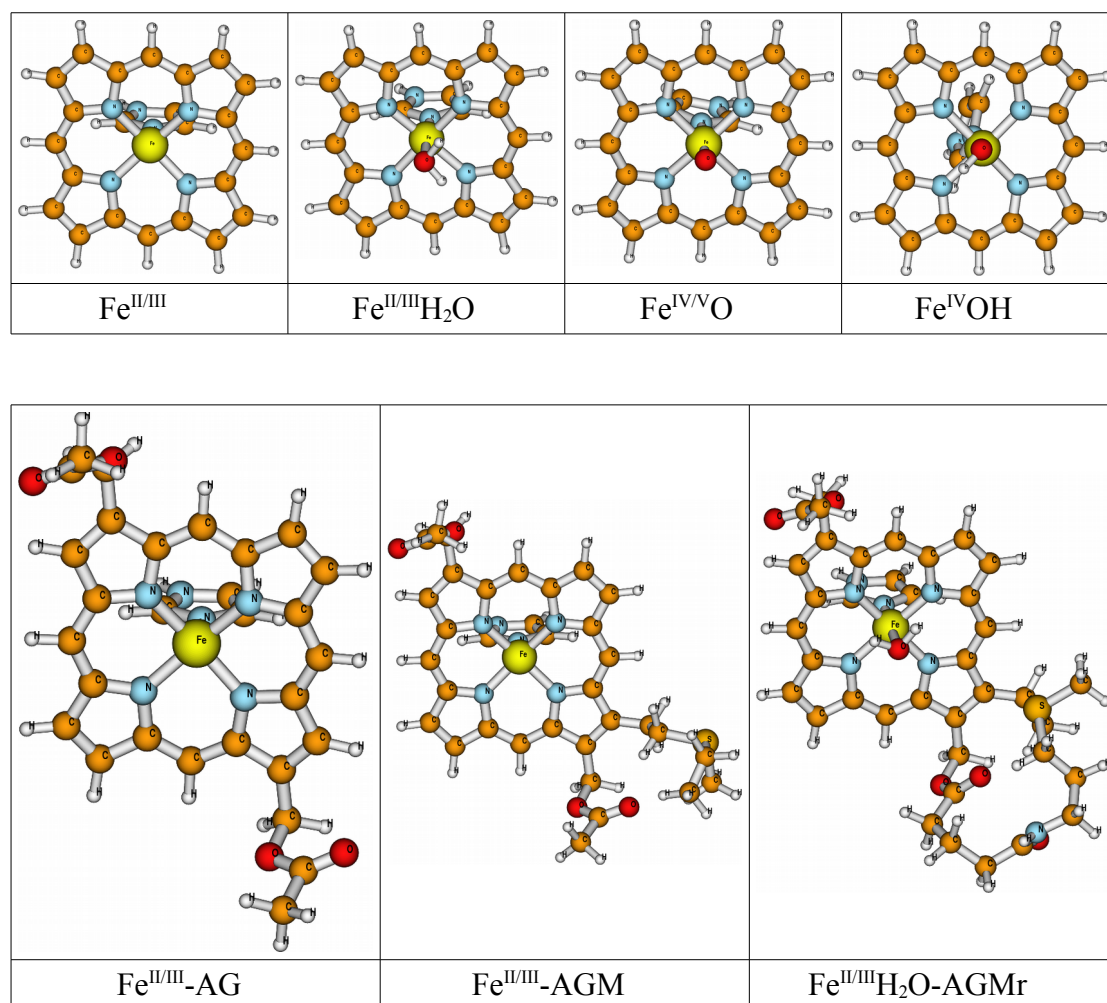**Figure 2.** Calculated spectra of the four resting-state models.

Figure 1.

Fe$^{II/III}$	Fe$^{II/III}$H$_2$O	Fe$^{IV/V}$O	Fe^{IV}OH

Fe$^{II/III}$-AG	Fe$^{II/III}$-AGM	Fe$^{II/III}$H$_2$O-AGMr

Figure 2.